Morphological Adaptation in an Energy Efficient Vibration-based Robot

Shiv Katiyar[1], Ghopy Kandasamy[1], Eranda Kulatunga[1], Md. Mustafizur[1], Fumiya Iida[2] and Surya G. Nurzaman[1]

***Abstract*— Morphological computation is a concept relevant to robots made of soft and elastic materials. It states that robot's rich dynamics can be exploited to generate desirable behaviors, which can be altered when their morphology is adapted accordingly. This paper presents a low-cost robot made of elastic curved beam driven by a motor, with morphological computation and adaptation ability. Simply by changing robot's shape and the rotating frequency of the motor that vibrates the robot's body, the robot is able to shift its behavior from showing a tendency to slide when it needs to perform tasks like going under confined space, to have more tendency to hop diagonally forward when the robot stands upright. It will also be shown that based on the proposed mechanism, the energy efficiency of the robot locomotion can be maximized.**

I. INTRODUCTION

Many types of robots were developed over the years for different purposes and tasks. Recently, the use of soft and elastic materials for developing robots have gained a lot of interest in the research area known as soft robotics [1], [2], [3], [4]. Due to the ability to flexibly deform, among others, it is expected that these robots will be able to accomplish tasks like locomotion in unstructured environments with energy efficient mobility, as well as go through debris and confined spaces. It is argued that the shared keyword of these "soft robots" is deformation, where the approaches to achieve it can include various technological solutions [5]. The examples include jamming with granular materials [6], silicone rubber with pneumatic actuation [7], tensegrity mechanism [8] as well as vibration and deformation of elastic beams [9].

In this regard, morphological computation is a biologically inspired concept relevant to soft robotics which argues that the body shape, material properties and physical dynamics of robots as physically embodied systems, can be exploited to generate desirable behavior during their interaction with the environment. The use of soft, deformable and elastic materials in robots is in many ways related to morphological computation due to these soft robot's complex dynamics [5], which will be altered when their morphology is varied [10], [11], [12]. For instance, one of the most actively investigated topics is the notion of variable stiffness actuator, i.e. the ability to adjust the stiffness of the robot's body through the implemented actuation method [13].

[1]Authors are with Mechanical Engineering Discipline, School of Engineering, Monash University, Malaysia shiv.katiyar@monash.edu, surya.nurzaman@monash.edu

[2]Fumiya Iida is with Machine Intelligence Laboratory, Department of Engineering, Cambridge University, Cambridge, United Kingdom fi224@cam.ac.uk

In terms of desirable characteristics of the robot that can be facilitated through the morphological computation concept, energy efficient locomotion is an example that attracts a lot of attention [14], [15], [16], [17]. Different types of locomotion that have been investigated from this perspective include hopping [14], running [15], [16] and walking [17].

The problem, however, pertains with regards to the lack of a systematic and low cost methodology to take advantage of the morphological computation and adaptation concept for having the desirable properties in robotic systems, such as adaptability or energy efficiency. From this perspective low cost lightweight yet dynamically complex robots composed of an elastic curved shaped beam and an attached rotating mass that vibrates the robot's body were proposed [9], [14], [18], [19]. It has been demonstrated that a C-shaped curved beam robot can perform stable and energy efficient hopping locomotion by exploiting the dynamics of the used elastic beam through the frequency of the rotation mass [14]. Other examples of research in this direction include the basic mechanism to generate different gait patterns [9] and goal directed motion by using a minimalistic control structure [9], [18], [19].

Due to the easy development, low cost nature and lightweight, energy efficiency as well as easily observable morphological computation ability, research on elastic curved beam robots can potentially be brought from fundamental ones to application-oriented ones like exploration or search and rescue scenarios where the this low cost and compliant robot is expected to be able to go under small openings. Nevertheless, an important aspect in this regard is the investigation of how the ability to adapt the morphology to the environment on-the-spot that affects the robot's dynamics and its desirable property such as energy efficiency.

The main goal of this paper is to do an initial investigation on how the morphological adaptation of curved beam robot affects its dynamics and energy efficiency for accomplishing potential tasks such as going under confined spaces. It will be shown that by simply changing its shape and the rotating frequency of the motor, the robot is able to shift its behavior from purely sliding when it needs to travel under confined space, to enable it to have more tendency to hop forward in the opposite condition. It will also be shown that based on the proposed mechanism, the energy efficiency of the robots motion can be maximized.

The rest of the paper will be organized as follows: first, in Section II, we introduce the structure and design of the curved beam robot used in the article. We use Lagrangian to develop a mathematical model of this robot to explain

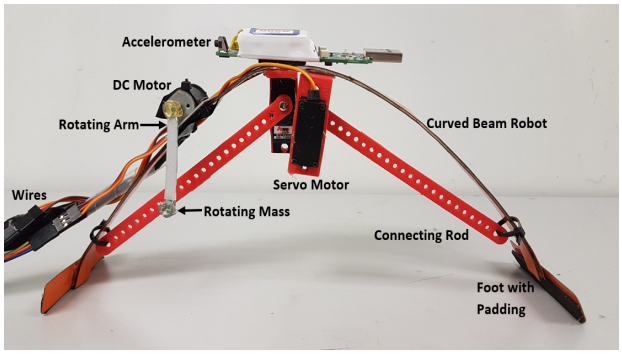

(a)

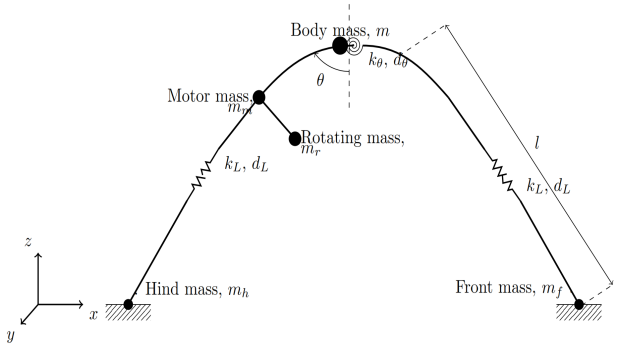

(b)

Fig. 1: Inverted U-shape curved beam robot (IUCBR). (a) Physical robot with all the components in place. (b) Equivalent schematic diagram of the physical robot.

the effect of vibrations during locomotion. In Section III, we explain the experimental setup used for the study and discuss about the robots energy efficiency. Then, Section IV describes experimental results and analyse the behaviour of the robot. Finally, we will conclude the paper and suggest several possible future works.

II. Curved Beam Robot with Shape Changing Ability

This section describes the design and modelling part of the curved beam robot in detail. As the shape of the robot is similar to inverted "U" so we call it the inverted U-shaped curved beam robot (IUCBR) here onwards. Later we explain the equivalent schematic diagram of the curved beam robot under study including the modeling of robot dynamics based on its shape changing ability.

A. Physical Robot

The inverted u-shape curved beam robot (IUCBR) described in this work consists of a flexible metal beam, or the body, rests on two horizontal metal strips at the either ends, as shown in Figure 1(a).

The robot is formed using two equal length steel strips which are stuck together using acrylic foam tape (shear strength $\geq$ 200gm/cm^2). Self-stability is ensured by designing the robot's structure properly, an approach that has already been verified earlier [9], [14]. In more details, the width of the robot feet is designed such that it is sufficient to balance the robot in sagittal plane and avoid it from falling. In addition, rubber from tyres of toy car are glued at the rear end of the feet to provide smoother motion and better grip.

We attach a DC motor with a small rotating mass on the upper part of rear leg of the robot, a Gulf Coast Data Concepts X200-4 USB impact accelerometer data logger at the top part of the robot body and two Power HD-1160A miniature servos placed under the joined strips. These servos are connected to the end part of robot body through cable-ties.

Figure 1(b) shows the schematic diagram of IUCBR with two links forming the legs of the robot and four point masses

TABLE I: Mechanical parameters of the Inverted U-shaped Curved Beam Robot (IUCBR)

Property	Value	Unit
Height of the robot	0.108, 0.124, 0.136	m
Length of the robot	0.183	m
Length of rotating mass	0.047	m
Mass of robot body	0.03913	kg
Mass of DC motor with the mount	0.02163	kg
Mass of the accelerometer	0.040	kg
Rotating Mass	0.00135	kg
Mass of IUCBR	0.12733	kg

at denoted by four dots. Point masses denote the distributed masses at a single point. Thus mass of hind foot, m_h and front foot, m_f is assumed to be at the bottom most point of the robot legs. The elastic metal strips forming the legs of the robot have been shown as longitudinal springs having stiffness k_L and damper with damping coefficients d_L. The rotational property of the elastic beam is placed in the centre at the top in form of torsional spring with stiffness k_θ and damping coefficient d_θ. The mass of the DC motor, m_m and the combined mass of two servo motors and accelerometer is placed at their equivalent respective position as on the physical robot. At the shaft end of the DC motor is attached a rotating arm and at the other of this arm is attached a rotating mass. The combined weight of these is is lumped and shown as rotating mas, m_r. The leg length is assumed to be l and these they make an angle θ, with the vertical.

B. Modeling of Robot Dynamics

We observe the structure of the physical robot and find out that the mass of the foot and the mass of the curved beam is negligible when compared to the mass of motors placed at the center point of robot body. Thus we model the dynamics of the robot based on Figure 1(b) as a mass spring system with the following assumptions for the ease of calculations:

- We analyse the locomotion in the sagittal plane where wider feet provide balance to the curved beam robot in frontal plane.

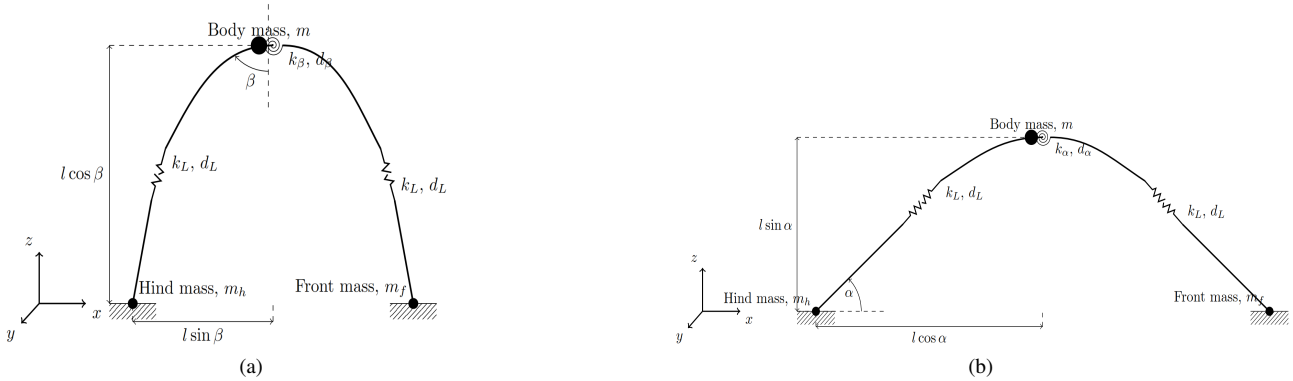

Fig. 2: Simplified schematic diagram of the inverted U-shape curved beam robot in two different configuration for dynamic modeling purpose. (a) IUCBR in Upright position when the angle with the vertical $\beta \approx 0$. (b) And, in the horizontal position when the angle with the horizontal $\alpha \approx 0$.

- We approximate the curved beam robot by three point masses, toe of them representing robot foot while the last one signifies mass of all the motors combined.
- After observing the behaviour of the IUCBR, the rotating ability in the body is represented by a torsional spring element placed at the centre top of the body while a linear spring element exhibits deflection in longitudinal direction is placed in the middle of the legs.
- The torsional and longitudinal stiffness coefficients of used mass spring system are linear and constant irrespective of the motion in the curved beam robot.

Applying the aforementioned assumptions to the schematic diagram of the IUCBR shown in Figure 1(b), we get the two configurations of inverted U-shaped curved beam robot in Figure 2(a) & (b) in a simpler arrangement.

Utilizing the shape changing ability of IUCBR, we vary the angle of the legs with the vertical, θ, in the range $\beta \leq \theta \leq (90^\circ - \alpha)$. Figure 2(a) shows IUCBR in upright position where its legs make an angle $\beta \approx 0$ with the vertical, mass of whole body, m, leg length, l, and longitudinal spring coefficient k_L and torsional spring coefficient k_β. Similarly, in the other configuration where the feet of IUCBR have a small angle α with the horizontal such that $\alpha \approx 0$. Rest of the robot parameters remain the same as mentioned in Figure 1(b). On the other hand, when robot makes an angle α with the horizontal surface its placed upon, the torsional spring coefficient is changed to k_α to remove the ambiguity while the longitudinal spring coefficient remains the same as earlier k_L. As a result, this model consists of mechanical design parameters (i.e., θ, l, l_0, m, k_L, k_β, k_α, d_L, d_β, d_α) and control parameters (i.e., α, β, m_r).

More specifically, the whole weight of the body is assumed to be concentrated at three point masses as shown which are connected through linear and torsional spring-damper elements. The energy supplied to the DC motor for the actuation of robot is rotational constant force which in turn gives the centripetal and centrifugal forces of the rotating mass.

To study the locomotion of vibration based robots, resonance frequency of the the structure in place is a key parameter [9], [14]. As in, if we are somehow able to induce vibrations in the structure that have frequency equal to the body then two frequencies get synchronised with one another and aid in achieving high performance. Since the body of IUCBR is made up of elastic material having tendency to stretch and rotate thus the structure has torsional and longitudinal frequencies of vibrations.

Now we aim to look closely at the two models in Figure 2 and analytically determine the expression for torsional and longitudinal resonance frequencies by estimating the Lagrangian $\mathcal{L}$ of the curved beam robot in the upright position:

$$\mathcal{L}_U = mgl\cos\beta + \frac{1}{2}m(l\beta)^2 + k_\beta(\beta-\beta_0)^2 + k_L(l-l_0)^2 \quad (1)$$

The torsional equation of motion is derived by differentiating $\mathcal{L}_U$ with respect to torsional angle β

$$\frac{d\mathcal{L}_U}{d\beta} = -mgl\sin\beta + ml^2\ddot{\beta} + 2k_\beta(\beta-\beta_0) \quad (2)$$

As we can see, for small angles $\sin\beta \approx \beta$ and the torsional resonance frequency of the curved bean robot is obtained using the homogeneous part of differentiation equation:

$$\ddot{\beta} + \omega_\beta^2\beta = 0 \quad (3)$$

Thus, torsional resonance frequency is found to be,

$$\omega_\beta = \sqrt{\frac{2k_\beta - mgl}{ml^2}} \quad (4)$$

Similarly to get the longitudinal resonance frequency we differentiate $\mathcal{L}_U$ with respect to leg length, l

$$\frac{d\mathcal{L}_U}{dl} = mg + m\ddot{l} + 2k_L(l-l_0) \quad (5)$$

on comparing with homogeneous part we get longitudinal resonance frequency as

$$\omega_L = \sqrt{\frac{2k_L}{m}} \quad (6)$$

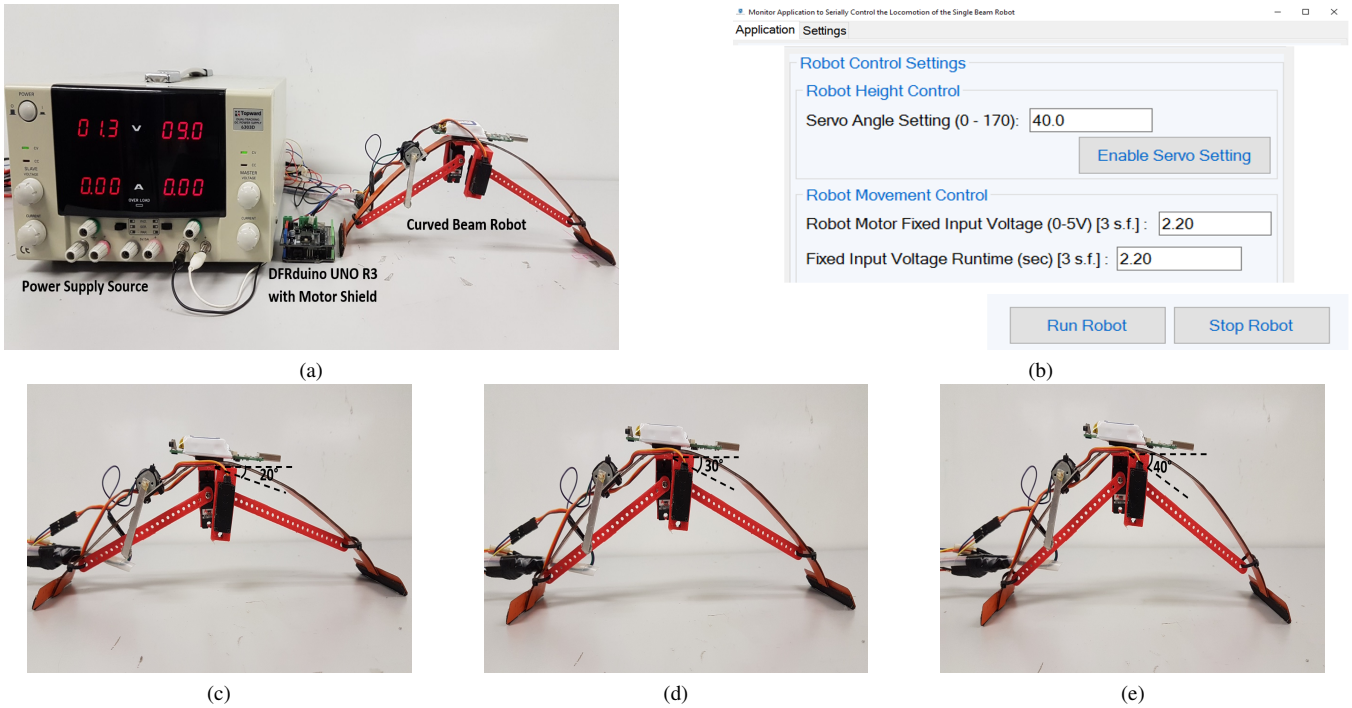

(a) (b) (c) (d) (e)

Fig. 3: Experimental setup. (a) IUCBR with DFRduino board and power supply for the board. (b) Software GUI to control the voltage for DC motor and servo motors. (c), (d) and (e) show the robot in different configurations of 20°, 30°and 40°. The angle is measured between the horizontal and the shaft connected to servo motor about the motor axis as shown in bottom row.

Similarly, on the same lines as for upright position we derive the Lagrangian $\mathcal{L}$ for robot with configuration parallel to horizontal ground and all the parameters retain their significance as before with the α being measure in anti-clockwise direction from the ground.

$$\mathcal{L}_H = mgl\sin\alpha + \frac{1}{2}m(l\alpha)^2 + k_\alpha(\alpha-\alpha_0)^2 + k_L(l-l_0)^2 \quad (7)$$

We obtain torsional resonance frequency as

$$\omega_\alpha = \sqrt{\frac{2k_\alpha + mgl}{ml^2}} \quad (8)$$

and, longitudinal resonance frequency as

$$\omega_L = \sqrt{\frac{2k_L}{m}} \quad (9)$$

The torsional and longitudinal resonance frequencies of the robot in horizontal i.e. 20°configuration and in upright configuration of 40°are recorded by fixing the robot to the table, tune the frequency and observe the maximum amplitudes at each corresponding direction, similar to the procedure explained in [14] over several times. The result is shown in Table II and for the clarity of text it's put under the section 4.B Analysis. It can be seen that in case of 40°configuration the torsional and longitudinal frequencies occur closer to each other when compared with 20°configuration as expected by the model.

III. Experimental Setup

In this section we give details about the experiment bench setup for this paper, as shown by Figure 3. Figure 3(a) shows the curved beam robot described in Section 2 placed on a particular surface to record the experimental data. An IBM table with the standard size of 1.5'W x 6'L x 2.5'H whose top is made of laminated high pressured board 18mm thick of grey color is used as surface to run the robot. When the DC motor is actuated with a constant power supply the small rotating mass, weighing 1.35gm that is attached at the end of the rotating arm which in turn is connected to the shaft of DC motor at one end, induces vibrations in the curved beam robot. When the rotating mass frequency approximates to the resonance frequency of the curved beam robot, the robot should move efficiently as the magnitude of the motion should be maximized with minimum used energy.

The energy efficiency of a robot can be studied very well with the help of accepted metric which is the specific resistance known as the cost of transportation (CoT) [14]. Following equation 10a shows how to calculate the cost of transport,

$$CoT = \frac{P}{mgv} \quad (10a)$$

A more usable form can be achieved by putting, power (P) as product of voltage (V) and current (I) and velocity (v) as ratio of distance (d) and time (t). Thus, converting equation 10a into:

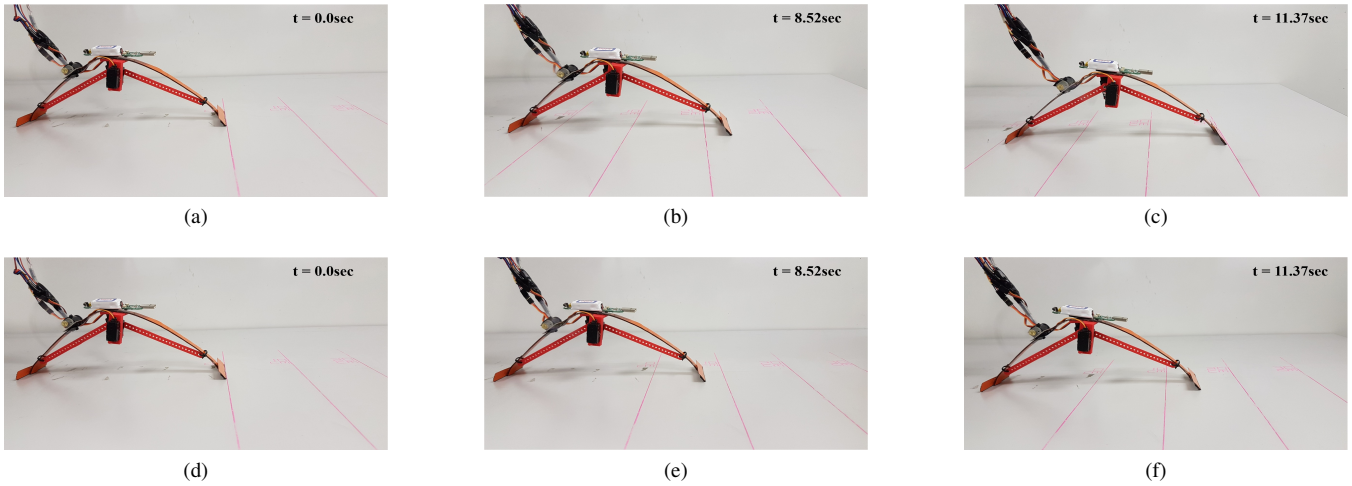

(a) (b) (c)

(d) (e) (f)

Fig. 4: Snapshots of IUCBR in motion in 30°configuration on experiment table with four straight lines drawn at spacing of 10cm each. For detailed view of the attained locomotion please refer to the video submitted.

$$CoT = \frac{VIt}{mgd} \tag{10b}$$

where m is total mass of system in kg, P is energy the expenditure in watts, g is standard gravitational acceleration in m/s^2 and v is velocity in m/s, V is applied voltage in volts, I is applied current in ampere, t is trail time duration of robot in run, m is the total mass of the system in kg, d is distance covered by the robot for the clocked time t in seconds.

It can therefore be seen that this setup helps in determining the energy efficiency of IUCBR by calculating CoT for different shapes. The data from accelerometer helps in stating that by changing the frequency of induced vibrations in the IUCBR we can control the locomotion behaviour or in other words the its energy consumption for better locomotion.

We use servo motors to change the shape of the curved beam robot which are controlled through a DFRduino UNO V3.0 board with motor shield. It is a simple microcontroller board fully compatible with Arduino UNO R3 and Arduino IDE open-source development environment. Figure 3(b) shows the GUI of the software used to control the servos which change the shape of the robot. In the images the servo angle had been set to 40°and an input voltage of 2.20V is fed to the DC motor. Figure 3(c), (d) and (e) show IUCBR in different shapes.

The X200-4 USB accelerometer data logger uses accelerometer sensor to record the raw digital data. Although this helps in minimizing processor load, increasing sample rate capability, and avoiding data errors due to floating point calculations this raw data needs to be processed to get the useful form. The 16-bit data having 2^{16} or 65536 discreet counts, covers the full range of the ±200g sensor. Thus, we divide the raw data by the conversion factor is 65536/(400*9.807) ≈ 16.706 or multiply by 0.05986 to get the value in m/s^2.

Next step is to convert this time domain data to frequency domain and obtain the magnitude of power coefficient in the direction of accelerometer axes. For each set of readings we find maximum power coefficient against corresponding frequency value. We also record the distance covered and time taken by the robot for that set of input voltage and current. For each set of data we calculate the mean and standard deviation of all the parameters of interest like input voltage, speed, cost of transport (CoT) and power.

As a final step we repeat the above whole process for the other two values of angle of configuration that decide the shape of the robot.

IV. Experimental Results and Analysis

In this section we show the results of the real-world robot as an output of the experiments carried out. Based on that we analyse the characteristics and behaviour of the IUCBR developed.

A. Results

The rear leg, on which motor with rotating mass is mounted, propels the robot to move forward. Once the DC motor is powered, its shaft rotates anti-clockwise such that the rotating mass provides forward momentum when rotating and induces vibrations in the rear part of the structure. The elastic nature of the steel strip propagates the forward momentum to the front leg, forcing the front leg to move forward. The rubber pads glued at the legs then enable this shift of vibrations into significant robot movement.

Figure 4 shows the running cycle of the robot in motion, on the experiment table with equally spaced lines drawn on it, under the effect of induced vibration by the DC motor in the robot body. The comparative snapshots show the robot at the starting line in (a) and (d) and timer at 0.0s, having different input voltages fed to the DC motor. The top row (a)-(c) shows the robot covering a distance of 30cm from the starting line in 11.37s. The speed of the robot was recorded

as 0.0263 m/s for input voltage 2.134V with CoT as 1.380. While, on the other hand bottom row (d)-(f) a slower moving robot with speed of 0.0164 m/s but registering the best and lowest CoT of 0.546 for input voltage of 0.891V.

The exhibited behaviour of locomotion of IUCBR can be described as following (also refer to the attached video): As the mass swings backwards, it forces the top of the robot to move backwards. This movement is pressuring the rear leg and thus lifting the front leg. At this moment, robot balances its total weight on the rear leg which tends to contract due to the elasticity of the metal and added body weight on itself. Stored energy in the rear leg releases as soon as the swinging mass is on the way to the front, which moves the robot forward while the front leg is still in the air. Thus, there is increment in flexing between the legs when compared with the robot in its still position. Similarly, when the rotating mass is swinging towards the front, the top of the robot will also swing towards the front switching the weight of the robot from the rear leg to the front leg and lifting the rear leg while storing energy in the front leg by contracting it. This movement will move the rear leg to the front.

Finally, as the rotating mass moves again towards the back of the robot, rear leg will touch the ground while the energy is stored in the front leg of the curved beam. The added rubber to the back of the rear leg gives added friction to the rear leg than of the front leg which results the front leg to slip and fling in to air while transferring the stored energy to the rear leg of the robot in the same time which the swing mass swings further behind of the robot and the total mass of the robot is again on the rear leg of the robot. This whole process makes the robot move to the front efficiently.

The plot of variation of CoT over the range of input voltage is shown in Figure 5 where we have three curves one each for a different configuration. The default shape of the robot is the one in which the angle of the connecting rod with the horizontal is 30°and we can see that we get the lowest value of CoT as 0.546 at input voltage 0.89V after which tends to increase till the voltage of 2.13V is achieved. Same is the case with 20°configuration where we get the lowest value of CoT as 0.708 against an input voltage of 1.01V which shows that even the robot with a deformed shape from it original body structure but tends to maintain the CoT near its best value. For the 40°robot configuration we get an inverted bell shape curve till voltage 1.80V after which it starts to drop in again indicating another value of two resonance frequencies for the structure. It records the lowest value of CoT as 0.727 for input voltage of 1.63V.

During the locomotion, the robot moves at different speeds at the best CoT registered for different configurations. For the 20°and 30°configuration where the robot is almost in horizontal position attains a speed of 0.0277m/s and 0.0264m/s for 1.008V and 0.891V as input voltage. While, in case of 40°or upright position, the IUCBR tends to move really quick logging speed of 0.0815m/s for 1.630V input voltage.

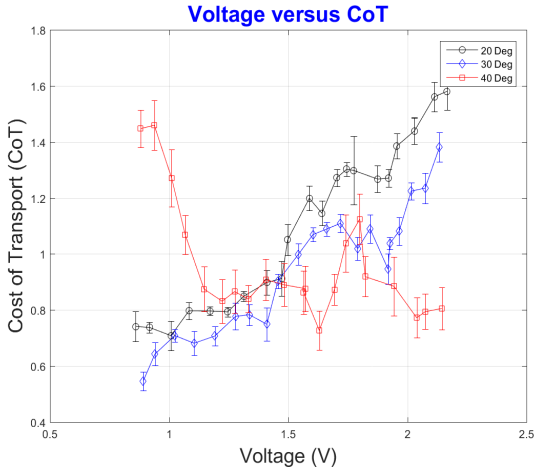

Fig. 5: Variation of CoT for IUCBR for three different configurations over the entire input voltage range.

B. Analysis

The detailed variation of CoT with respect to voltage and speed for robot snapshots showed in Figure 4 is plotted in Figure 5. The concept of morphological computation and the exploitation of the body-environment dynamics dictates this occurrence strengthening the fact that resonance frequency of the structure is the main cause of energy efficient locomotion.

Figure 6 depicts the value of power coefficients in the two principal axes directions for the three different robot configurations against the set of values which record the best CoT in each of the cases. As mentioned in Section 3, these power coefficients are obtained by applying FFT on converted accelerometer data. It shows the magnitude of the power of acceleration in two principal axes; frontal plane along x-axis, and sagittal plane along z-axis. For the purpose of clarity, the power in the axial plane along the y axis is not shown in Fig 6 as it simply shows the sideways vibrations which are not the centre of discussion in analyzing the robot behaviour.

We observe that when the power in the x and z direction are quite different, and x is higher, it implies that only the longitudinal frequency drives the robot as shown in Figure 6(a) and (b) and again supported by the values of torsional and longitudinal frequencies recorded experimentally in Table II. Physically, it means that the robots will have more tendency to slide forward with maximum power. While, the power in x and z direction are close to each other when the robot is close to upright position, which indicates that both the torsional and longitudinal frequencies occur at approximately the same time as shown in Figure 6(c) and this is also the case as evident from Table II. Physically, it means that the robot has more tendency to hop diagonally forward motion as the power at x and z direction are almost the same with a resultant in x-z direction. The observations made in Figure 6 are similar to what has been shown by the model in 7. Figure 6(c) is more similar to the model in Figure 7(a), meaning that the torsional and longitudinal frequencies

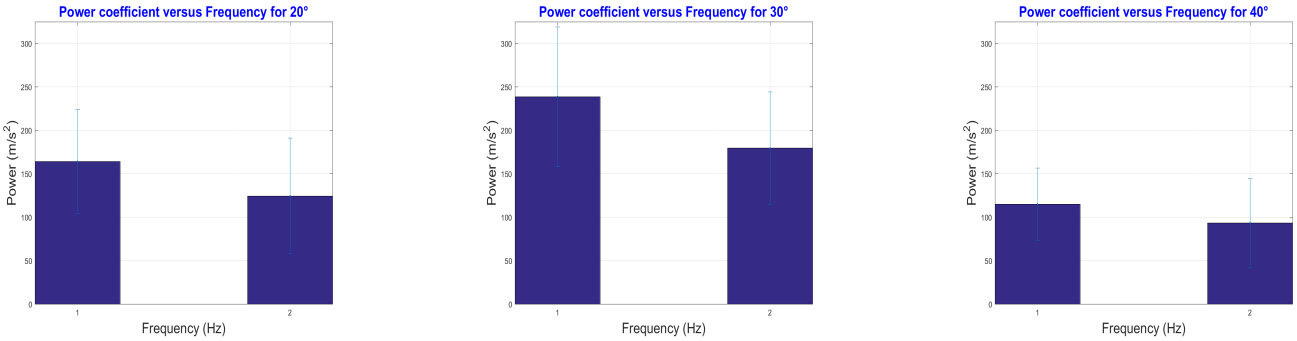

(a) (b) (c)

Fig. 6: Maximum Power coefficients for 20°, 30°and 40°along x (as denoted by 1) and z (as denoted by 2) axes. The ratio of powers in these two axes, P_x/P_z, are 1.33, 1.32 and 1.22 respectively for the aforementioned configurations.

(a) (b)

Fig. 7: Inverted U-shape curved beam robot in two different configuration indicating acting dominant forces that drive the locomotion through the ratio of the power coefficients. (a) When the robot is in the horizontal position, its tendency is to slide forward with power in x axis dominating the power in the z axis. (b) And, when the robot is in upright position it has more tendency to diagonally hop forward as the power in x axis and z axis are more balanced. The ratio P_x/P_z shown here is taken from the results shown in Figure 6.

TABLE II: Torsional and Longitudinal frequencies for IUCBR in two configurations along with the corresponding spring constants derived by the model explained in subsection 2.2. The number in the bracket shows the normalized values.

Robot Configuration	Torsional Frequency, ω_T (Hz)	Torsional spring constant, k_θ (Nm/rad)	Longitudinal Frequency, ω_L (Hz)	Longitudinal spring constant k_L (N/m)
40°	23.386	18.906 (1)	19.315	462.158 (1.111)
20°	25.148	22.512 (1.191)	11.611	415.862 (1)

are placed close to each other. Figure 6 (a) & (b) show much similar behavior to what is modelled in Figure 7(b), when the torsional and longitudinal frequencies are separated, while longitudinal frequency has much lower value.

If we compare the torsional and longitudinal frequency of the two configurations stated in Table II we observe that in the 40°configuration the frequencies are further apart while in the 20°configuration ω_β and ω_α have much closer values. In the horizontal, i.e. 20°configuration, torsional frequency is 25.148 Hz and longitudinal frequency 11.611 Hz while in the upright configuration, or 40°, the observed torsional frequency is 23.386 Hz and longitudinal frequency is 19.315 Hz. Experimental values of torsional and longitudinal frequencies in Table II and the power coefficient values in Figure 6 support each other and help in explaining the energy efficiency and gait behavior. For example, when the robot is almost horizontal as shown by Figure 2(b), the lowest COT shown by Figure 5(a) happens when the robot is driven by a very low frequency. Here, based on Figure 6 & 7, the behavior of the robot is to simply slide forward. The COT and gait behavior make sense as the derived model shows that for this shape the longitudinal resonance frequency should be more separated with, and lower than, the torsional one. At this frequency, robot slides forward with maximum power and maximizes the energy efficiency.

V. Conclusion

This paper proposes a unique morphologically adaptive legged robot based on curved beam which requires no complex control structure that can potentially accomplish practical tasks like going through confined spaces while maintaining its energy efficiency. Due to its shape changing ability, the robot is able to take advantage of the body environment dynamics resulting from the induced frequency eventually leading to highly energy-efficient locomotion. The robot is developed with simple design and fabrication method which is also light weight and very low in cost. Our experimental results with the proposed curved beam robot design show the lowest recorded value of cost of transportation (CoT) as 0.546, without any further processing such as taking offset of the energy consumed by DC motor under no load condition. This result is comparable with other robots which show comparatively similar speed but are much heavier when compared with IUCBR like curved beam robot [14] and ARL Monopod II [20].

As a future work for this preliminary investigation, we plan to investigate several aspects. First, being the effect of collision with the ground which is indispensable for the energy efficiency in the generated gait. So, we aim to study this effect in detail. We also aim to describe the rotating mass and its effect on the robot's overall dynamics. The effects of torsional and longitudinal resonance frequencies are very important and are obvious from the results in paper but the dynamical effect of the rotating mass is also a key factor. Lastly, we plan to perform further numerical analysis such as comparison with simulation results of the model.

ACKNOWLEDGMENT

The authors would like to thank Maninda Andradi for helping in developing basic structure of the IUCBR and Sheng Hong Cuwa for his assistance in data collection. Shiv Katiyar is supported by Merit Scholarship Monash University Malaysia. The authors acknowledge the support of the FRGS Grant (Project no: FRGS/1/2017/ICT02/MUSM/03/3) provided by the Ministry of Higher Education (MOHE), Malaysia, and the School of Engineering Seed Funding (2016), Monash University Malaysia.

References

[1] Cecilia Laschi and Matteo Cianchetti. Soft robotics: new perspectives for robot bodyware and control. *Frontiers in bioengineering and biotechnology*, 2:3, 2014.

[2] Daniela Rus and Michael T Tolley. Design, fabrication and control of soft robots. *Nature*, 521(7553):467–475, 2015.

[3] Surya G Nurzaman, Fumiya Iida, Cecilia Laschi, Akio Ishiguro, and Robert Wood. Soft robotics [tc spotlight]. *IEEE Robotics & Automation Magazine*, 20(3):24–95, 2013.

[4] Nurzaman, Surya G and Iida, Fumiya and Margheri, Laura and Laschi, Cecilia. Soft robotics on the move: scientific networks, activities, and future challenges. *Soft Robotics*, 1(2): 154–158, 2014.

[5] Liyu Wang, Surya G. Nurzaman, and Fumiya Iida. Soft-material robotics. *Foundations and Trends in Robotics*, 5(3):191–259, 2017.

[6] Erik Steltz, Annan Mozeika, Nick Rodenberg, Eric Brown, and Heinrich M Jaeger. Jsel: Jamming skin enabled locomotion. In *IROS 2009. IEEE/RSJ International Conference on*, pages 5672–5677. IEEE, 2009.

[7] Robert F Shepherd, Filip Ilievski, Wonjae Choi, Stephen A Morin, Adam A Stokes, Aaron D Mazzeo, Xin Chen, Michael Wang, and George M Whitesides. Multigait soft robot. *Proceedings of the National Academy of Sciences*, 108(51):20400–20403, 2011.

[8] Kyunam Kim, Adrian K Agogino, Deaho Moon, Laqshya Taneja, Aliakbar Toghyan, Borna Dehghani, Vytas SunSpiral, and Alice M Agogino. Rapid prototyping design and control of tensegrity soft robot for locomotion. In *Robotics and Biomimetics (ROBIO), 2014 IEEE International Conference on*, pages 7–14. IEEE, 2014.

[9] Murat Reis, Xiaoxiang Yu, Nandan Maheshwari, and Fumiya Iida. Morphological computation of multi-gaited robot locomotion based on free vibration. *Artificial life*, 19(1):97–114, 2013.

[10] Fumiya Iida and Surya G Nurzaman. Adaptation of sensor morphology: an integrative view of perception from biologically inspired robotics perspective. *Interface Focus*, 6(4):20160016, 2016.

[11] Stefano Mintchev and Dario Floreano. Adaptive morphology: A design principle for multimodal and multifunctional robots. *IEEE Robotics & Automation Magazine*, 23(3):42–54, 2016.

[12] Hideyuki Ryu, Yoshihiro Nakata, Yutaka Nakamura, and Hiroshi Ishiguro. Adaptive whole-body dynamics: An actuator network system for orchestrating multijoint movements. *IEEE Robotics & Automation Magazine*, 23(3):85–92, 2016.

[13] Sebastian Wolf, Giorgio Grioli, Oliver Eiberger, Werner Friedl, Markus Grebenstein, Hannes Höppner, Etienne Burdet, Darwin G Caldwell, Raffaella Carloni, Manuel G Catalano, et al. Variable stiffness actuators: Review on design and components. *IEEE/ASME transactions on mechatronics*, 21(5):2418–2430, 2016.

[14] Murat Reis and Fumiya Iida. An energy-efficient hopping robot based on free vibration of a curved beam. *IEEE/ASME Transactions on Mechatronics*, 19(1):300–311, 2014.

[15] Fabian Guenther and Fumiya Iida. Energy-efficient monopod running with a large payload based on open-loop parallel elastic actuation. *IEEE Transactions on Robotics*, 2016.

[16] Sangok Seok, Albert Wang, Meng Yee Michael Chuah, Dong Jin Hyun, Jongwoo Lee, David M Otten, Jeffrey H Lang, and Sangbae Kim. Design principles for energy-efficient legged locomotion and implementation on the mit cheetah robot. *IEEE/ASME Transactions on Mechatronics*, 20(3):1117–1129, 2015.

[17] K. Hosoda M. Ogino and M. Asada. Learning energy-efficient walking with ballistic walking in adaptive motion of animals and machines. *International Conference on. Springer*, (AMAM 2006):435–454, 2006.

[18] Surya G Nurzaman, Xiaoxiang Yu, Yongjae Kim, and Fumiya Iida. Guided self-organization in a dynamic embodied system based on attractor selection mechanism. *Entropy*, 16(5):2592–2610, 2014.

[19] SG Nurzaman, X Yu, Y Kim, and F Iida. Goal-directed multimodal locomotion through coupling between mechanical and attractor selection dynamics. *Bioinspiration & biomimetics*, 10(2):025004, 2015.

[20] Mojtaba Ahmadi and Martin Buehler. The arl monopod ii running robot: Control and energetics. In *Robotics and Automation, 1999. Proceedings. 1999 IEEE International Conference on*, volume 3, pages 1689–1694. IEEE, 1999.